Rapid Synthesis and Screening of $Zn_xCd_{1-x}S_ySe_{1-y}$ Photocatalysts by Scanning Electrochemical Microscopy

Guanjie Liu,[†] Chongyang Liu, and Allen J. Bard*

Center for Electrochemistry, Department of Chemistry and Biochemistry, The University of Texas at Austin, Austin, Texas 78712, United States

Received: June 23, 2010; Revised Manuscript Received: October 15, 2010

Quaternary-alloyed $Zn_xCd_{1-x}S_ySe_{1-y}$ arrays were prepared from four precursor aqueous/glycerol (3:1) solutions with a robotic piezoelectric dispenser on fluorine-doped tin oxide (FTO) conductive glass. Hydrazine (N_2H_4) was used for protecting the selenium source, dimethylselenourea, from oxidation so that fabrication of the arrays could be carried out under ambient air conditions. The absorption spectra of the photocatalyst spots (230-μm size) on the array were measured with a fiber-optic/CCD detector system. The band gaps were a function of the elemental composition and ranged from 1.8 to 3.6 eV. The photoelectrochemical properties were evaluated by scanning electrochemical microscopy in the photoelectrochemical mode using an optical fiber tip attached to a Xe lamp as the excitation source. The spot with a precursor composition $Zn_{0.3}Cd_{0.7}S_{0.8}Se_{0.2}$ (elemental ratio, 1:2.12:1.75:0.81) showed the highest photocurrent under 150 W Xe lamp irradiation. The difference of the photocurrent onset indicated that addition of Zn raises the conduction band position of CdS_ySe_{1-y}.

1. Introduction

Photoelectrochemical (PEC) systems based on semiconductor electrodes are currently the most efficient chemical systems for the conversion of solar energy to electricity or fuels. For example, photoelectrochemical water splitting has been proposed as a means of using sunlight to produce hydrogen for use as a fuel, following the suggestion over 30 years ago that TiO_2 might be useful for this purpose.[1,2] A key factor in the fabrication of a PEC system is finding an appropriate light-absorbing electrode material (often called the photocatalyst). The ideal electrode material should have an appropriate band gap so that it can absorb visible light, have appropriately located conduction and valence band edge positions to carry out the desired reactions, and be stable under irradiation. Many semiconductor materials have been investigated as photocatalysts.[3−8] Among them, II−VI semiconductors such as ZnS, CdS, CdSe have been extensively investigated.[9−11]

There has been recent activity in attempting to vary or tune the semiconductor band gap by various doping or composition variation schemes, thus improving the light absorption properties and performance. Although much of this effort has focused on oxide semiconductors, II−VI semiconductors based on S and Se are of interest because they are characterized by a wide range of band gaps and lattice constants, making them suitable for applications in optoelectronic devices and biolabels.[12−14] Recently, quaternary-alloys of $Zn_xCd_{1-x}S_ySe_{1-y}$ were synthesized, and the band gap of these materials could be controlled by tuning the composition so that it was tunable across the entire visible spectrum.[15,16] Although many new photocatalytic materials based on II−VI binary semiconductors, such as Ni-doped ZnS,[17] $Zn_xCd_{1-x}S$,[18,19] $AgInS_2$−ZnS,[20] and CdS/TiO_2,[21] have been prepared by doping, making solid solutions, and constructing heterojunctions, to the best of our knowledge, there have been no reports on photoelectrochemical measurements of $Zn_xCd_{1-x}S_ySe_{1-y}$ or approaches to optimizing these materials.

Combinatorial methods based on automated synthesis and screening provide a rapid and systematic method for developing new photocatalysts. They have been applied, for example, to search for phosphors, sensors, and fuel cell catalysts.[22,23] Several groups have also employed combinatorial methods for searching the multielement space for oxide photocatalysts.[24−26] For example, our group has reported the screening of new photocatalysts by scanning electrochemical microscopy (SECM), with oxides, such as Pd/Fe, Sn/Fe, Ag/Fe, and Zn/In oxide.[27−30] We extend this approach here with nonoxide catalysts, in which we describe the rapid preparation of a quaternary alloy $Zn_xCd_{1-x}S_ySe_{1-y}$ spot array and investigation of their photoelectrochemical properties by SECM. The band gap of the spots was controlled by tuning the composition. We also report a method of measuring the optical absorbance spectra of the spots on the array using a simple home-built apparatus.

2. Experimental Section

Chemicals. F-Doped tin oxide (FTO)-coated glass was obtained from Pilkington Glass (Toledo, OH). Squares (15 mm $\times$15 mm) were cleaned by sonicating them successively in ethanol and isopropyl alcohol and rinsing with deionized water. $Zn(NO_3)_2$ (Aldrich), $Cd(NO_3)_2$ (Aldrich), thiourea (Alfa Aesar), dimethylselenourea (Strem), hydrazine (Aldrich), and glycerol (Fisher) were used as received for the preparation of array spots, and Milli-Q water was used to prepare all solutions. All metal precursor solutions were made with a 3:1 solution of water/glycerol with a metal salt concentration of 0.1 M, and the concentrations of thiourea and dimethylselenourea solution (containing 0.05 M hydrazine) were 0.2 M.

Preparation of Photocatalyst Arrays. A CH Instruments model 1550 dispenser (Austin, TX) used to fabricate the photocatalyst arrays consists of a stepper-motor-operated *XYZ* stage with a piezodispenser (MicroJet AB-01-60, MicroFab,

* To whom correspondence should be addressed. E-mail: ajbard@mail.utexas.edu.

† On leave from the State Key Laboratory of Multiphase Flow in Power Engineering, Xi'an Jiaotong University, Xi'an, 710049 China.

10.1021/jp1058116
Published on Web 11/15/2010

Plano, TX) attached to the head. The system was connected and controlled through a PC computer. The substrate (FTO) was placed under the piezodispenser tip, and the *XYZ* stage moved the dispenser head in a preprogrammed pattern while programmed voltage pulses were applied to the dispenser to eject the requested number of drops (~100 pL each) of the metal precursor solution onto the substrate. The first component (metal precursor solution) was loaded and dispensed in a preprogrammed pattern onto the FTO substrate. After flushing and washing the piezodispenser, the second component was loaded into the dispenser and dispensed into the existing pattern. The step was repeated when a third component was added. The relative number of drops of each metal salt component (~10 total) determined the spots' cation composition. In addition, thiourea and dimethylselenourea solutions were added into the spots with different ratios, and their total drop number was 5 to maintain the molar ratio of cations and anions as 1. Then the samples were mixed with a Vortex Genie 2 (Fisher, Pittsburgh, PA). Finally, the arrays were kept at 100 °C for 12 h under an argon atmosphere. For convenience, we report the precursor element ratio to denote the spots in the array. However, the actual compositions of the final compounds are different from the precursor amounts due to factors such as differential loss of selenide.

Screening the Spot Arrays. A schematic of the SECM setup has been shown in our previous paper.[27] A 400 μm optical fiber (FT-400-URT, 3M, St. Paul, MN) connected to a 150 W xenon lamp via a model 9091 five-axis fiber aligner (New Focus, San Jose, CA) was attached to the tip holder of a CHI model 900B SECM. The array was placed in a SECM cell made of Teflon with the FTO/photocatalyst working electrode array exposed at the bottom through an O-ring. A Pt wire and an Ag/AgCl electrode were used as counter and reference electrodes, respectively, and a 0.1 M Na_2SO_4/Na_2S solution was used as the electrolyte. Light from a 150 W xenon lamp was passed through the optical fiber, which was positioned perpendicular to the working electrode surface and illuminated onto the working electrode. A 420 nm long-pass filter was used to block the UV in visible light illumination experiments. The optical fiber tip was held and scanned 100 μm above the working electrode surface while a potential bias was applied to the working electrode array. The photocurrent produced during the scan was recorded and displayed as a two-dimensional image. The applied potential was −0.4 V vs Ag/AgCl.

Preparation and Measurement of Photoelectrochemical Properties of Bulk Spot Array Electrodes. Bulk spot array electrodes were fabricated on FTO-coated glass with a CH Instruments model 1550 dispenser in which all the spots had the same composition. The patterned bulk spot array electrodes were kept at 100 °C for 12 h. The electrochemical cell comprised a bulk spot array electrode, Ag/AgCl, and Pt wire as photoanode, reference electrode, and counter electrode, respectively. The photoanode was illuminated with a Xe lamp (150 W) equipped with a UV cutoff filter ($\lambda \geq 420$ nm). The photocurrent vs potential ($i-V$) response was measured in a 0.1 M Na_2SO_4/0.1 M Na_2S solution under UV−vis or visible light irradiation ($\lambda \geq 420$ nm).

Characterization. X-ray diffraction (XRD) measurements were performed with a Bruker-Norius D8 advanced diffractometer. The Cu K radiation source was operated at 40 kV and 40 mA. All measurements were carried out in the ($\theta/2\theta$) mode. Samples for XRD were prepared on a glass slide using the same solution as used to fabricate the arrays. HR-TEM images were obtained with a JEOL 2010F transmission electron microscope.

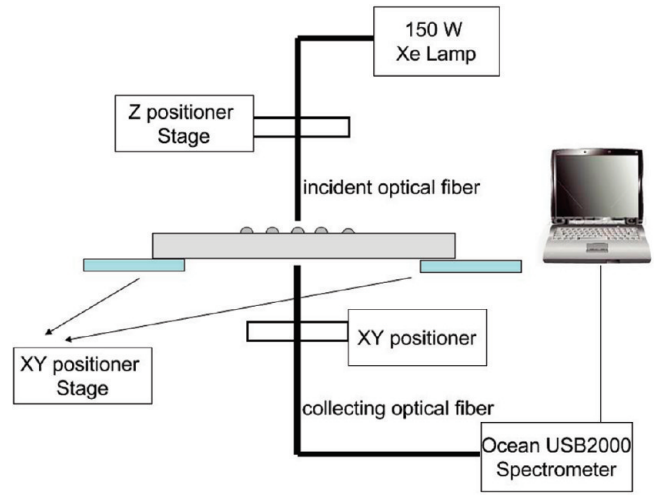

Figure 1. Diagram of the setup for light absorption measurements of the arrays.

The elemental analysis was carried out using a LEO 1530 scanning electron microscope equipped with an energy disperse spectroscopy (EDS) system. UV−vis absorption spectra of the array were measured using a home-built absorption spectrometer. Figure 1 is the schematic diagram of the setup. The incident light came from a 200 μm optical fiber connected to a 150 W Xe lamp, and an Ocean Optics USB2000 fiber optic spectrometer was used to measure the light intensity. The measurement range was 350−1000 nm; however, because the UV part of the incident light was very weak, the measurement might have some error for the material with a larger band gap (>3.0 eV). The surface profile of the array was measured using a Veeco NT-9100 optical profiler.

3. Results and Discussion

SECM Studies on the Zn−Cd−S−Se System. For rapidly investigating the PEC activity of the quaternary semiconductor $Zn_xCd_{1-x}S_ySe_{1-y}$, we prepared the spot array as shown in Figure 2a and screened it using SECM. The array had 10 rows, numbered from top to bottom. The ratio of Zn/Cd varied from 10/0 to 0/10 in every two rows as a cycle and repeated five times, so the left spot in rows 1, 3, 5, 7, and 9 contained only Zn^{2+}, and the rightmost spot in rows 2, 4, 6, 8, and 10 contained only Cd^{2+}. The ratio of S/Se varied continuously from the first cycle (5/0) to the fifth cycle (0/5), so the top left corner and the bottom right corner in the pattern were pure ZnS and CdSe, respectively, and the last spot in the second row and the first spot in the ninth row were CdS and ZnSe. Other spots were ternary or quaternary compounds with different compositions varying regularly across the array. A photograph of the as-prepared array is shown in Figure 2b. The color of the spots varied from transparent to dark, providing a qualitative indication of the amount of light absorbed by the spots as the elemental composition varied. Figure 2c and d show the SECM images under UV−vis and visible light irradiation, respectively, in a 0.1 M Na_2SO_4/Na_2S solution as the electrolyte and the array held at −0.4 V vs Ag/AgCl. The $Zn_{0.3}Cd_{0.7}S_{0.8}Se_{0.2}$ spot showed the highest activity under both UV−vis and visible light irradiation, where the photocurrent attained 1.27 and 0.78 μA, respectively. In the first and third cycles, $Zn_{0.3}Cd_{0.7}S$ and $Zn_{0.3}Cd_{0.7}S_{0.6}Se_{0.4}$ also showed higher photocurrent than pure CdS and $CdS_{0.6}Se_{0.4}$, respectively, indicating that addition of Zn can improve the photoactivity of CdS_ySe_{1-y}. This phenomenon is consistent with previous reports.[31] The photocurrent of

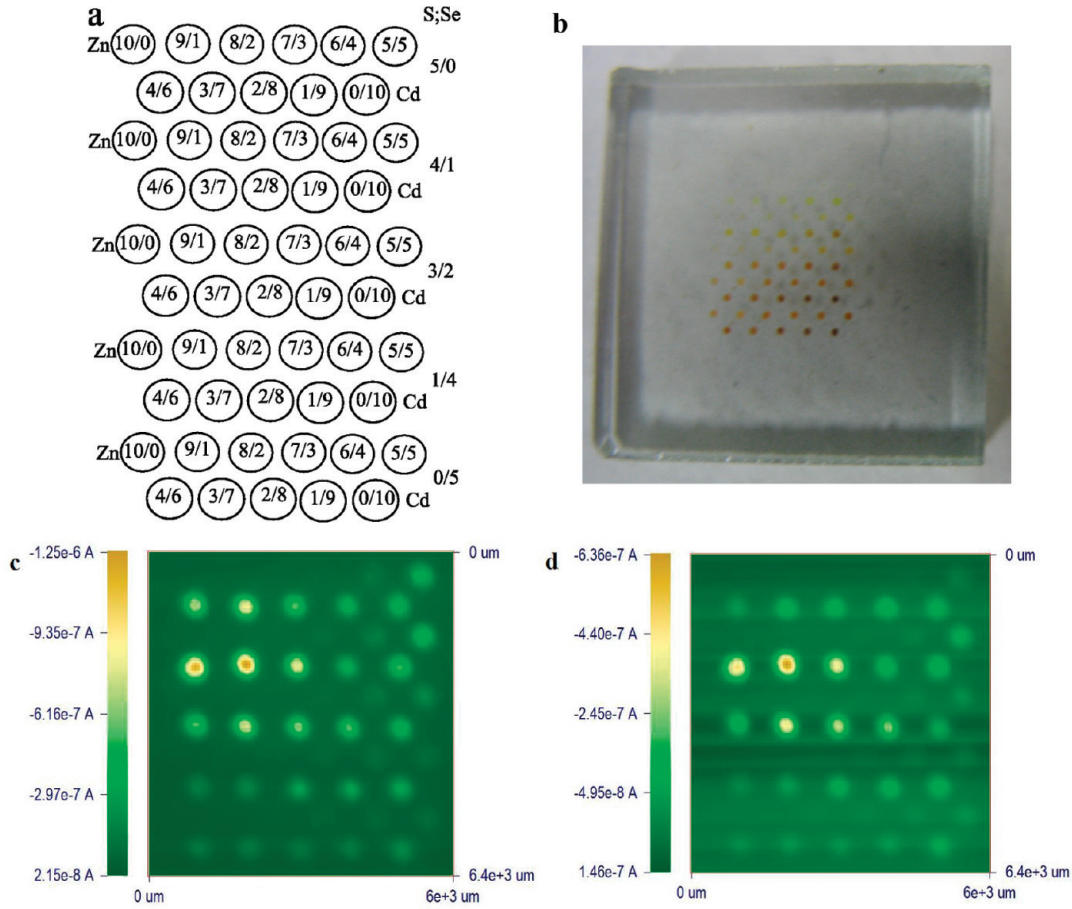

Figure 2. (a) Dispensed pattern of $Zn_xCd_{1-x}S_ySe_{1-y}$ array; (b) photograph of $Zn_xCd_{1-x}S_ySe_{1-y}$ array sample; (c) (d) SECM images of the array photocurrent in a 0.1 M Na_2SO_4/Na_2S solution with the array held at −0.4 V vs Ag/AgCl with (c) UV−vis and (d) visible light irradiation.

$Zn_{0.4}Cd_{0.6}S_{0.8}Se_{0.2}$ under UV−vis light irradiation was close to that of $Zn_{0.3}Cd_{0.7}S_{0.8}Se_{0.2}$, but its photocurrent under visible light was obviously lower. This difference suggests that $Zn_{0.3}Cd_{0.7}S_{0.8}Se_{0.2}$ has a smaller band gap, E_g, and can absorb more visible light.

The causes of the changed behavior upon doping or addition of different metals and anions to a given photocatalyst is complicated. The most obvious is changes in the band gap, which results in differences in light absorption. However, changes in carrier mobility and passivation of recombination centers in the bulk and on the surface can play a role. For the case of interest here, the predominant effect is the band structure and E_g. ZnS and CdS have similar crystal structures and should form solid solutions. The presence of Zn would increase E_g and shift the conduction band edge compared with CdS.[31] The addition of selenium (as found for CdS−CdSe systems) causes a decrease in E_g.

Characterization of the Array. Figure 3 shows the XRD patterns of $Zn_xCd_{1-x}S$ samples formed via pyrolysis of a sample prepared from a mixed solution that was the same as those used in the preparation of the array. The patterns indicate that all the materials possessed a cubic structure. As the Zn^{2+} content increased, the diffraction peaks shifted toward the higher-angle side compared with the pattern of pure CdS. This shift is consistent with the ionic radius of Cd^{2+} (0.97 Å) being larger than that of Zn^{2+} (0.74 Å). This also indicates that Zn^{2+} entered into the framework of CdS and formed a solid solution. Broad XRD peaks are attributed to the absence of long-range order in the materials and imply a small particle size. From the half-width of the XRD peaks, the average particle size of CdS was

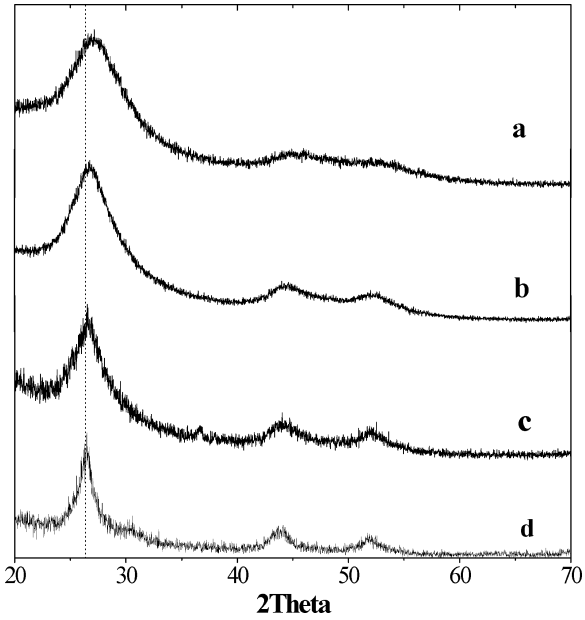

Figure 3. XRD patterns of the samples on glass slide substrates prepared by the drop-cast method: (a) $Zn_{0.8}Cd_{0.2}S$, (b) $Zn_{0.6}Cd_{0.4}S$, (c) $Zn_{0.4}Cd_{0.6}S$, and (d) CdS.

estimated to be ∼5.8 nm based on the Scherrer equation. The composition of the spots was measured by EDS. Table 1 shows the EDS result of $Zn_{0.5}Cd_{0.5}S_ySe_{1-y}$. The ratios of Zn/Cd are in accordance with the precursor ratio (1:1). However, the ratio of S/Se is much lower than the precursor ratio. On the other hand, the ratio of cations (Zn + Cd) to anions (S + Se) is higher

TABLE 1: The Elemental Composition of $Zn_{0.5}Cd_{0.5}S$, $Zn_{0.5}Cd_{0.5}S_{0.8}Se_{0.2}$, $Zn_{0.5}Cd_{0.5}S_{0.6}Se_{0.4}$, $Zn_{0.5}Cd_{0.5}S_{0.2}Se_{0.8}$, and $Zn_{0.5}Cd_{0.5}Se$ Spots in the Array Measured by EDS

spot	Zn/Cd/S/Se
$Zn_{0.5}Cd_{0.5}S$	1:1.07:1.45:0
$Zn_{0.5}Cd_{0.5}S_{0.8}S_{0.2}$	1:1.05:1.01:0.54
$Zn_{0.5}Cd_{0.5}S_{0.6}Se_{0.4}$	1:0.97:0.58:0.93
$Zn_{0.5}Cd_{0.5}S_{0.2}Se_{0.8}$	1:1.03:0.23:1.66
$Zn_{0.5}Cd_{0.5}Se$	1:1.07:0:1.97

than 1:1, suggesting sulfur loss occurred during the synthetic process. This might cause vacancies or replacement by oxygen that cannot be determined by EDS because of the strong O signal from the FTO substrate.

Figure 4 shows the HR-TEM image of CdS. The sample was prepared by dipping the copper grid directly into a $Cd(NO_3)_2$ and thiourea mixed solution that was held at 100 °C in an Ar atmosphere for 12 h. We would expect the sample's morphology to be essentially the same as the material in the array. As shown in the figure, the material consisted of large aggregates of nanoparticles. The average diameter of the nanoparticles was ~5 nm, which agrees with the calculated result using the Scherrer equation. This size is sufficiently small that the properties of the materials in the spots might be affected by quantum effects.

The absorption spectra were measured with the fiber optic/CCD setup described in the Experimental Section. Figure 5 shows the absorption spectra of some of the spots in the array. The absorption edge of CdS, $Zn_{0.3}Cd_{0.7}S_{0.8}Se_{0.2}$, and CdSe spots annealed at 100 °C showed the main onset of light absorption at 480, 530, and 680 nm, respectively. In the array, the CdSe spot had the smallest band gap, showing a blue shift in the absorption edge when the Se was substituted by sulfurs, producing a larger E_g. Substitution of Zn for Cd had a similar effect on the absorption spectrum. The absorption edge of the nanoparticulate CdS and CdSe was blue-shifted compared with the standard absorption spectra of bulk CdS (2.4 eV, 516 nm) and bulk CdSe (1.7 eV, 730 nm) reported previously,[32,33] consistent with a quantum effect in the ~5 nm particles. As shown in Figure 5, compared with CdS and CdSe spots annealed at 100 °C, CdS and CdSe spots annealed at 450 °C had a red shift and the absorption edge moved to about 530 and 740 nm, which are close to the bulk values.

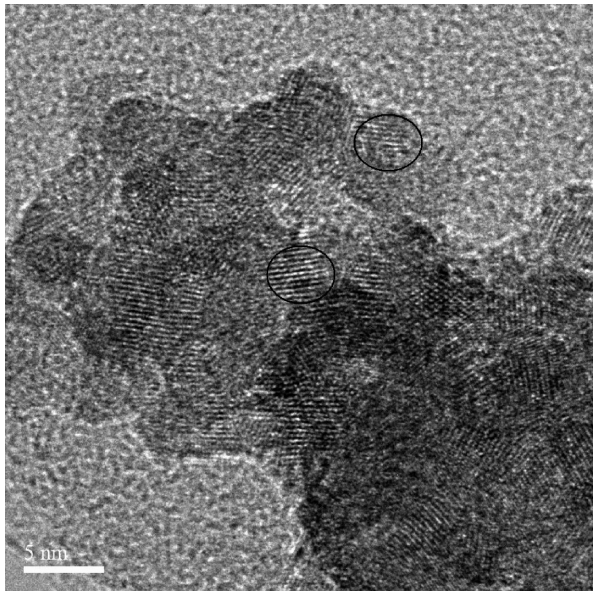

Figure 4. HR-TEM image of CdS sample made by dipping the copper grid into the mixed $Cd(NO_3)_2$ and thiourea precursor solution and then treating in the same way as the array.

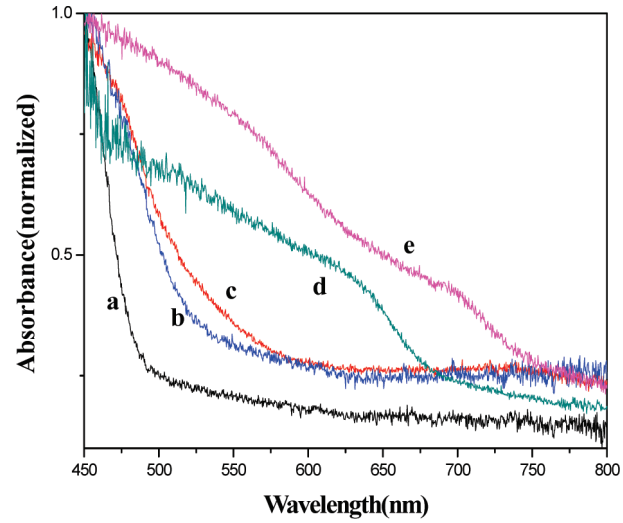

Figure 5. Absorption spectra of (a) CdS spot, (b) CdS spot annealed at 450 °C, (c) $Zn_{0.3}Cd_{0.7}S_{0.8}Se_{0.2}$ spot, (d) CdSe spot, and (e) CdSe spot annealed at 450 °C.

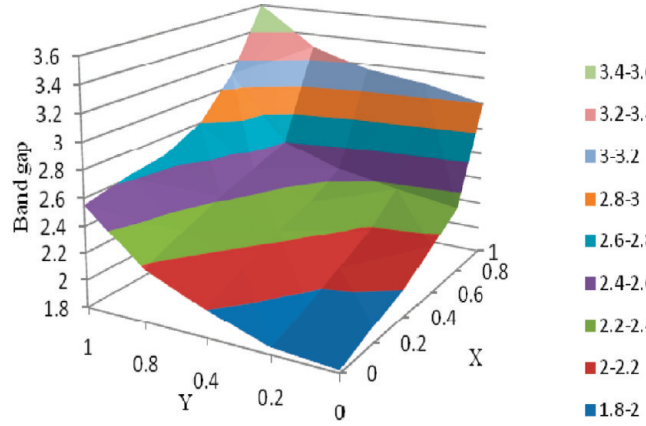

Figure 6. Three-dimensional profile of $Zn_xCd_{1-x}S_ySe_{1-y}$ arrays' band gap as a function of x and y.

A plot of estimated band gap values as a function of composition is shown as a 3-dimensional plot in Figure 6. The band gap value was calculated according to the equation $\alpha h\nu = A(h\nu - E_g)^{1/2}$ (where α, $h\nu$, and E_g were the absorption coefficient, the discrete photon energy, and the band gap energy, respectively; A is a constant). These are given in a table in the Supporting Information. Because of limitations in the Xe lamps' spectrum range and detector range, it was difficult to obtain the absorption spectra of wide-band-gap materials, such as ZnS, so the bulk E_g of ZnS (3.6 eV) was used in Figure 6, making estimates for nanoparticles with values above ~3 eV somewhat uncertain. Note that qualitatively, the band gap of the spots increased monotonically as the content of Zn and S increased in the spots.

Photoelectrochemical Measurements on Bulk Films. After the optimized material was found using the SECM array measurements, it was necessary to make a bulk film to confirm its photoelectrochemical properties in a larger cell. The nature of a larger film of a given material is often dependent on the method of preparation (e.g. spin coating, drop coating, spray, CVD, or PVD). Therefore, we prepared bulk spot array electrodes, which consisted of 25 identical spots prepared with

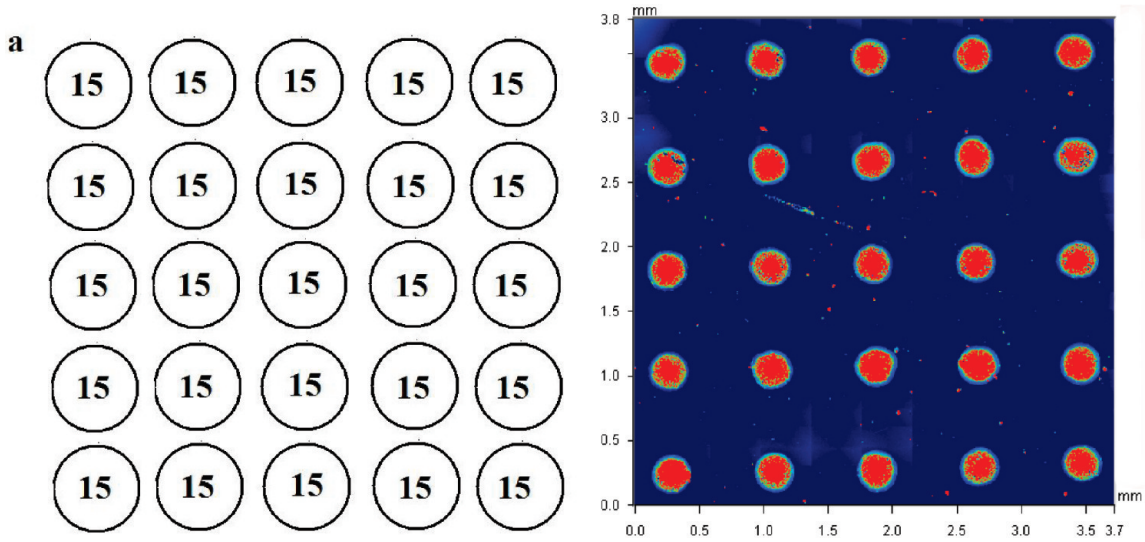

Figure 7. (a) The dispensed pattern of the 25-spot films. (b) The optical surface profile of the $Zn_{0.3}Cd_{0.7}S_{0.8}Se_{0.2}$ 25-spot array.

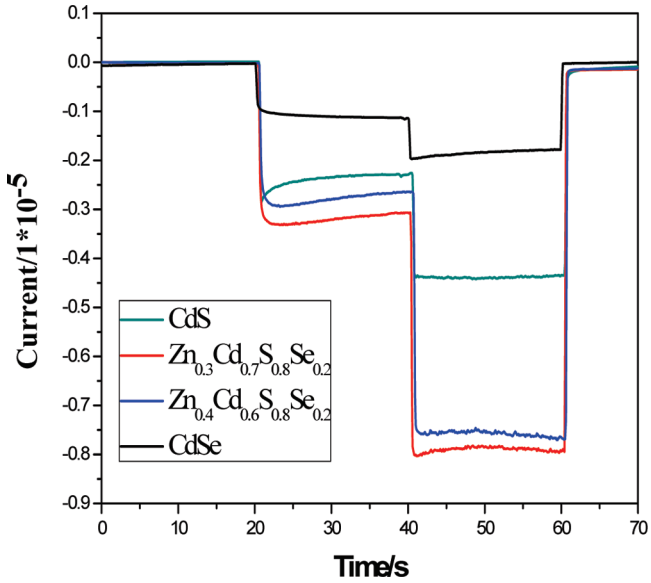

Figure 8. Current−time transient response of CdS, $Zn_{0.3}Cd_{0.7}S_{0.8}Se_{0.2}$, $Zn_{0.4}Cd_{0.6}S_{0.8}Se_{0.2}$, and CdSe 25-spot arrays in the dark (0−20 and 60−70 s), and under visible (20−40 s) and UV−vis (40−60 s) light irradiation.

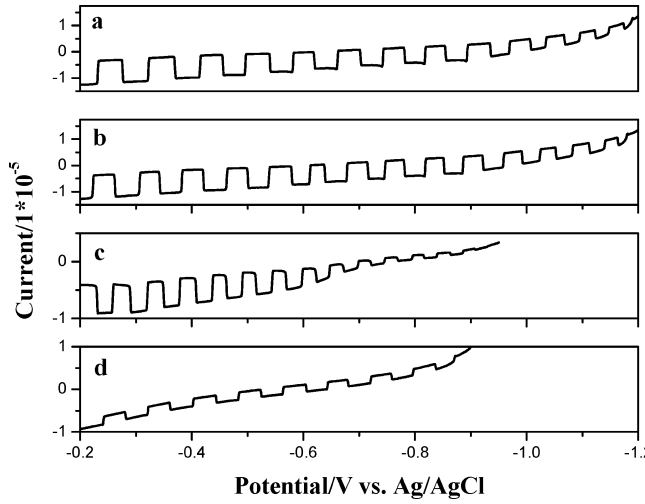

Figure 9. Chopped photocurrent−potential curves of (a) $Zn_{0.3}Cd_{0.7}S_{0.8}Se_{0.2}$, (b) $Zn_{0.4}Cd_{0.6}S_{0.8}Se_{0.2}$, (c) CdS, and (d) CdSe 25-spot arrays under UV−vis light irradiation.

the dispenser and treated using the same procedures as that for the multicomposition array (Figure 7a). Each bulk array's precursor composition was the same as that corresponding to the spot in the array shown in Figure 2. The size and thickness of the $Zn_{0.3}Cd_{0.7}S_{0.8}Se_{0.2}$ bulk spot array electrode is shown in Figure 7b, as obtained with the optical profiler. All of the spots had a uniform thickness (~440 nm) and diameter (~230 μm), indicating that the dispenser preparation method is quite reproducible. The response in SECM PEC screening is somewhat dependent on the spot diameter, since the fiber optic illuminates a larger area than the spot size, so size reproducibility is important in array preparation.

The photocurrents of CdS, $Zn_{0.4}Cd_{0.6}S_{0.8}Se_{0.2}$, $Zn_{0.3}Cd_{0.7}S_{0.8}Se_{0.2}$, and CdSe 25-spot array electrodes are compared in Figure 8. $Zn_{0.3}Cd_{0.7}S_{0.8}Se_{0.2}$ showed the best photoactivity under both UV−vis and visible light irradiation. CdSe showed the lowest photocurrent, and most of the photocurrent under UV−vis light (1.6 μA) was contributed by visible light absorption (1.1 μA), consistent with the small band gap of CdSe. The relative photoactivities of different electrodes agree with the screening results.

Figure 9 shows chopped photocurrent−potential curves of the bulk spot array electrodes. The photocurrent onsets, approximately indicating the open circuit photo potentials, of CdS and CdSe electrodes are located at about −0.95 and −0.9 V vs Ag/AgCl in a 0.1 M Na_2S aqueous solution (~pH 12.7), respectively. However, the photocurrent onset of the $Zn_{0.3}Cd_{0.7}S_{0.8}Se_{0.2}$ electrode almost reached −1.2 V vs Ag/AgCl. This suggests the conduction band position of CdS is slightly higher than that of CdSe, consistent with its origin primarily with Cd^{2+}, in agreement with previous results.[34] The effect of Zn in $Zn_{0.3}Cd_{0.7}S_{0.8}Se_{0.2}$ results in a higher conduction band edge position compared with CdS and CdSe, perhaps the origin of the improved photoactivity.

4. Conclusions

We have demonstrated a technique for rapid preparation, screening, and optical absorption measurement of quaternary-alloyed $Zn_xCd_{1-x}S_ySe_{1-y}$ materials. First, rapid preparation was realized by making a spot array on FTO coated glass using the robotic piezoelectric dispenser. Hydrazine provided an oxygen-

free environment in the precursor solution and allowed the preparation of the array to be performed under ambient air conditions without oxidation of dimethylselenourea. The array was then screened by SECM, and the optimum composition $Zn_{0.3}Cd_{0.7}S_{0.8}Se_{0.2}$ for the best photoactivity was found. The absorption spectra of the array were measured and the continuous shift of the absorption spectra showing that the spots band gap was controlled by tuning the spots composition. The optimum composition was also confirmed by testing the multispot array electrode photoelectrochemical properties.

Acknowledgment. This material is based upon work supported by the Department of Energy under award number DE-SC0002219 and the Robert A. Welch Foundation (F-0021). G.L. thanks the National Scholarship Fund of the China Scholarship Council for support and advisor Prof. Liejin Guo from Xi'an Jiaotong University. Helpful discussions with Fu-Ren F. Fan are also gratefully acknowledged.

Supporting Information Available: Additional information as noted in text. This material is available free of charge via the Internet at http://pubs.acs.org.

References and Notes

(1) Bard, A. J.; Fox, M. A. *Acc. Chem. Res.* **1995**, *28*, 141.
(2) Honda, K.; Fujishima, A. *Nature* **1972**, *238*, 37.
(3) Zou, Z.; Ye, J.; Sayama, K.; Arakawa, H. *Nature* **2001**, *414*, 625.
(4) Kato, H.; Asakura, K.; Kudo, A. *J. Am. Chem. Soc.* **2003**, *125*, 3082.
(5) Maeda, K.; Teramura, K.; Lu, D.; Takata, T.; Saito, N.; Inoue, Y.; Domen, K. *Nature* **2006**, *440*, 295.
(6) Khaselev, O.; Turner, J. A. *Science* **1998**, *280*, 425.
(7) Asahi, R.; Morikawa, T.; Ohwaki, T.; Taga, A. Y. *Science* **2001**, *293*, 269.
(8) Wang, X.; Maeda, K.; Thomas, A.; Takanabe, K.; Xin, G.; Carlsson, J. M.; Domen, K.; Antonietti, M. *Nat. Mater.* **2009**, *8*, 76.
(9) Reber, J. F.; Meier, K. *J. Phys. Chem.* **1984**, *88*, 5903.
(10) Mau, A. W.-H.; Huang, C.; Kakuta, N.; Bard, A. J.; Campion, A.; Fox, M. A.; White, M. J.; Webber, S. E. *J. Am. Chem. Soc.* **1984**, *106*, 6537.
(11) Smotkin, E. S.; Cervera-March, S.; Bard, A. J.; Campion, A.; Fox, M. A.; Mallouk, T.; Webber, S. E.; White, J. M. *J. Phys. Chem.* **1987**, *91*, 6.
(12) Bruchez, M.; Morrone, P.; Gin, S.; Weiss, S.; Alivisatos, A. P. *Science* **1998**, *281*, 2018.
(13) Klimov, V. I.; Mikhailovsky, A. A.; Xu, S.; Malko, A.; Hollingsworth, J. A.; Leatherdale, C. A.; Eisler, H. J.; Bawendi, M. G. *Science* **2000**, *290*, 314.
(14) Park, H.; Barrelet, C. J.; Wu, Y.; Tian, B.; Qian, F.; Lieber, C. M. *Nat. Photonics* **2008**, *2*, 622.
(15) Pan, A.; Liu, R.; Sun, M.; Ning, C. *J. Am. Chem. Soc.* **2009**, *131*, 9502.
(16) Deng, Z.; Yan, H.; Liu, Y. *J. Am. Chem. Soc.* **2009**, *131*, 17744.
(17) Kudo, A.; Sekizawa, M. *Catal. Lett.* **1999**, *58*, 241.
(18) Kakuta, N.; Park, K. H.; Finlayson, M. F.; Ueno, A.; Bard, A. J.; Campion, A.; Fox, M. A.; Webber, S. E.; White, J. M. *J. Phys. Chem.* **1985**, *89*, 732.
(19) Liu, G.; Zhao, L.; Ma, L.; Guo, L. *Catal. Commun.* **2008**, *9*, 126.
(20) Tsuji, I.; Kato, H.; Kobayashi, H.; Kudo, A. *J. Am. Chem. Soc.* **2004**, *126*, 13406.
(21) Sun, W.; Yu, Y.; Pan, H.; Gao, X.; Chen, Q.; Peng, L. *J. Am. Chem. Soc.* **2008**, *130*, 1124.
(22) Wang, J.; Yoo, Y.; Gao, C.; Takeuchi, I.; Sun, X.; Chang, H.; Xiang, X.-D.; Schultz, P. G. *Science* **1998**, *279*, 1712.
(23) Danielson, E.; Golden, J. H.; Mcfarland, E. W.; Reaves, C. M.; Weinberg, W. H.; Wu, X. D. *Nature* **1997**, *289*, 944.
(24) Woodhouse, M.; Herman, G. S.; Parkinson, B. A. *Chem. Mater.* **2005**, *17*, 4318.
(25) Woodhouse, M.; Parkinson, B. A. *Chem. Mater.* **2008**, *20*, 2495.
(26) Kleiman-Shwarsctein, A.; Hu, Y.; Forman, A. J.; Stucky, G. D.; McFarland, E. W. *J. Phys. Chem. C* **2008**, *112*, 15900.
(27) Lee, J.; Ye, H.; Pan, S.; Bard, A. J. *Anal. Chem.* **2008**, *80*, 7445.
(28) Jang, J. S.; Yoon, K. Y.; Xiao, X.; Fan, F.-R. F.; Bard, A. J. *Chem. Mater.* **2009**, *21*, 4803.
(29) Jang, J. S.; Lee, J.; Ye, H.; Fan, F.-R. F.; Bard, A. J. *J. Phys. Chem. C* **2009**, *113*, 6719.
(30) Liu, W.; Ye, H.; Bard, A. J. *J. Phys. Chem. C* **2010**, *114*, 1201.
(31) Xing, C.; Zhang, Y.; Yan, W.; Guo, L. *Int. J. Hydrogen Energy* **2006**, *31*, 2018.
(32) Jing, D.; Guo, L. *J. Phys. Chem. B* **2006**, *110*, 11139.
(33) Nair, M. T. S.; Nair, P. K.; Pathirana, H. M. K. K.; Zingzra, R. A.; Meyers, E. A. *J. Electrochem. Soc.* **1993**, *140*, 1987.
(34) Lee, Y.; Chi, C.; Liau, S. *Chem. Mater.* **2010**, *22*, 922.

JP1058116